Cellular therapy after spinal cord injury using neural progenitor cells

Vroemen, Maurice

Chapter 6

In vivo high resolution MRI of neuropathological changes in the injured rat spinal cord

Am. J. Neuroradiol. in press

Thomas Weber[#]
Maurice Vroemen[#]
Volker Behr
Thomas Neuberger
Peter Jakob
Axel Haase
Gerhard Schuierer
Ulrich Bogdahn
Cornelius Faber
Norbert Weidner
[#] These authors contributed equally to this work.

ABSTRACT

Magnetic resonance imaging (MRI) is the most comprehensive means to assess structural changes in injured central nervous system (CNS) tissue in humans non-invasively over time. The few published *in vivo* MRI studies of spinal cord injury in rodent models using field strengths up to 7 T suffer from low spatial resolution, flow, and motion artifacts. The aim of this study was to assess the capacity of a 17.6 T imaging system to detect pathological changes occurring in a rat spinal cord contusion injury model *ex vivo* and *in vivo*. Therefore seven adult female Fischer 344 rats received a contusion injury at thoracic level Th 10, which caused a severe and reproducible lesion of the injured spinal cord parenchyma. From 2 to 58 days post-injury, high-resolution MRI was performed *ex vivo* (n=2) or *in vivo* in anesthetized rats (n=5 spinal cord injured + 1 intact control animal) using 2D multi-slice spin and gradient echo imaging sequences, respectively, combined with electrocardiogram triggering and respiratory gating. The acquired images provided excellent resolution and gray/white matter differentiation without significant artifacts. Signal changes, which were detected with *ex vivo* and *in vivo* MRI following spinal cord injury, could be correlated with histologically defined structural changes such as edema, fibroglial scar and hemorrhage. These results demonstrate that MRI at 17.6 T allows high-resolution structural analysis of spinal cord pathology after injury.

1. INTRODUCTION

Magnetic resonance imaging (MRI) represents a powerful means to non-invasively visualize pathomorphological changes in humans following spinal cord injury [1, 2]. MRI findings correlate with histopathological sequela observed after spinal cord injury such as edema, hemorrhage and secondary degenerative changes such as cyst formation. Moreover, MRI allows to predict the severity of neurological deficits after spinal cord injury [3]. On an experimental level, regenerative strategies have been validated in animal models of spinal cord injury, which promote functional and structural recovery. In particular, cell based transplantation strategies hold great promise in regenerating the injured spinal cord [4-10]. Ultrastructural restoration in animals is primarily assessed by post mortem microscopical analysis of spinal cord parenchyma. In order to be able to monitor regenerative strategies in clinical applications, non-invasive imaging techniques are mandatory. Only animal studies allow the direct correlation of in vivo MRI data with histological post mortem data as a prerequisite for proper interpretation of MRI findings in human studies after therapeutic interventions. Anatomical structures that must be resolved in mice or rats are five to ten times smaller than in humans. This implies that volume elements in imaging data are smaller by a factor of roughly 100 to 1000. MRI studies of the spinal cord of rodent models, wide-

ly used to assess the efficacy of regenerative strategies following spinal cord injury, require a sufficiently high signal-to-noise ratio (SNR) in order to resolve small-scale structures with satisfactory contrast. Furthermore, respiratory motion and blood flow may induce image artifacts. Structural changes occurring after spinal cord injury such as edema, cystic defects, atrophy and hemorrhage have been detected in several MRI based in vivo studies. [11-18] [19]. However, partial volume effects resulting from a lower spatial resolution in these studies reduced the reliability to exactly allocate and interpret signal changes seen with MRI. Furthermore, studies demonstrating an acceptable spatial resolution employed implantable coils, which as opposed to surface coils require an additional invasive procedure. In the present study, we investigated, whether high field MRI at 17.6 T would allow superior spatial resolution and thus improved detection of structural changes in the adult rat spinal cord following a defined contusion injury ex vivo and in vivo.

2. MATERIALS AND METHODS

2.1 Animals

The spinal cord injury and imaging experiments were conducted using young adult female Fisher 344 rats (n=8) weighing 160-180g. *Ex vivo* MRI was performed in 2 spinal cord injured animals, *in vivo* MRI in 5 spinal cord injured (Table 1) and 1 uninjured rat. All experiments were carried out in accordance with the European Communities Council Directive (86/609/EEC) and institutional guidelines for animal care. All efforts were made to minimize the number of animals used, as wells as their suffering.

2.2 Surgical procedures

For the surgical procedure animals underwent anesthesia made up of a mixture of ketamine (62.5mg/kg body weight; WDT, Garbsen, Germany), xylazine (3.175mg/kg body weight; WDT, Garbsen, Germany) and acepromazine (0.625mg/kg body weight, Sanofi-Ceva, Düsseldorf, Germany) in 0.9% sterile saline solution. Rats received spinal cord contusion injuries using the Infinite Horizon (IH) spinal cord injury device (Precision Systems & Instrumentation, Lexington, USA) as previously described [20]. A laminectomy was performed at thoracic level Th 10 to expose the dorsal portion of the spinal cord. The animals were suspended by attaching Adson forceps to the rostral Th 9 and caudal Th 11 vertebral bodies. Particular care was taken to align the exposed spinal cord perpendicular to the axis of the Impactor. The 2.5 mm stainless steel impounder tip was lowered to approximately 3–4 mm above the surface of the exposed spinal cord. The contusion injury was finally induced by applying an impact force of 2 Newton (equals 200 kilodyne) to the exposed spinal cord at a velocity of 130 mm/sec. Overlying muscle layers were sutured and the skin was closed. Postoperatively, animals were kept warm, placed on beds of sawdust and given manual bladder evacuation twice per day for a period of up to 10 days as necessary and received intramuscular injections of 10

mg Cotrimoxazol (Ratiopharm, Ulm, Germany) once daily for a period of 10 days. Animals regained automatic neurogenic bladder function after 5 to 10 days.

2.3 MR scanner

All MR imaging experiments were conducted on a vertical Bruker 750 wide bore magnet system (Bruker Biospin, Rheinstetten, Germany) at 17.6 T with a bore size of 89 mm.

2.4 In vivo MR imaging

Anesthesia was induced by inhalation of 4% isoflurane and maintained with 2% isoflurane in carbogen (95% oxygen and 5% carbon dioxide). Body temperature was maintained by heating the gradient cooling unit to 37 ± 2°C.

A total of 5 rats underwent in vivo MRI between 2 and 58 days after thoracic spinal cord contusions were applied (Table 1). An uninjured rat with an intact spinal cord served as control. An animal gradient system with 57 mm inner diameter and 0.2 T/m was used. Due to space restrictions within the gradient system, imaging of the rat spinal cord in wide bore magnets was not possible with commercially available hardware. Therefore, a probehead and surface coil were custom-built to provide maximum space for adult rats as described [21]. The surface coil was designed as a transmit-receive coil in a half-cylindrical carrier mounted on an optimized probebase. The probebase included balancing units (baluns), which are important at higher frequencies due to the increased sensitivity of the electrical setup to imbalances.

To avoid artifacts caused by blood flow and respiratory motion a triggering unit (RAPID Biomedical, Wuerzburg, Germany) for combined electrocardiogram (ECG) triggering and respiratory gating was used.

A multi-slice 2D spoiled gradient echo sequence was used with a TE around 4 ms, depending on the exact spatial resolution used, and a TR around 200 ms depending on the heart rate. Up to 9 slices were acquired per scan. Using surface coils, gradient echo sequences are advantageous for transmission, as they are far less sensitive to radio frequency (RF) inhomogenities. Two interleaved multi-slice data sets were acquired to cover a full 3D volume. The spatial resolution was at least 78 x 78 µm in-plane with a slice thickness of 370 µm in axial slices and 156 x 98 µm in-plane with a slice thickness of 370 µm in sagittal slices. Each series took between 15 and 20 minutes.

2.5 Ex vivo MR imaging

For ex vivo MRI, one animal was perfused at 2 weeks and another animal at 4 weeks after the contusion injury with 150 ml cold 0.1 M phosphate buffered saline (PBS) followed by 400 ml 4% paraformaldehyde in PBS. Spinal cords were removed and post fixed overnight in 4% paraformaldehyde in PBS and then left for 1 day in PBS containing 30% sucrose at 4°C. This fixation procedure is required for the histological evaluation following ex vivo MRI. For the actual imaging process, spinal cord specimens were transferred into 5 mm wide

Table 1: *Time table of in vivo MRI scans for each individual animal.*

animal #	1. MRI scan (days post-injury)	2. MRI scan (days post-injury)	3. MRI scan (days post-injury)	Histology
1	18	25	39	no[1]
2	18	25	39[3]	no[1]
3	6	38	58	no[1]
4	2	38	--	yes[2]
5	2	13[4]	58[5]	yes[2]

[1] animals died during or shortly after last MRI scanning procedure.

[2] animals sacrified one day after the last MRI scan.

[3] illustrated in Fig. 5

[4] illustrated in Fig. 4A-C

[5] illustrated in Fig. 4D-F

NMR tubes (Wilmad, Buena, NJ, USA) filled with PBS containing 30% sucrose. Air bubbles were removed from the tube using a vacuum pump and leaving each sample at a pressure of approximately 50 mbar for around 10 minutes.

A gradient system with 1 T/m and an inner diameter of 40 mm was used with a commercial 5 mm linear birdcage resonator as transmit- and receive coil. The sample was kept at 20±1°C during imaging experiments.

Positioning of the sample was performed using a 3D low-resolution gradient echo sequence. A 2D multi-slice spin echo with an echo time (TE) of 7.5 ms, a repetition time (TR) of 2 s, 24 signal averages (NA), and a total scan time 3.5h was used. With a field of view (FOV) of 6 x 6 mm and an acquisition matrix of 256 x 256, the spatial resolution was 23 x 23 µm in-plane with a slice thickness of 300 µm. A total of 30 slices was acquired in axial direction and 14 slices in sagittal direction.

2.6 Histology

Animals were transcardially perfused with a 0.9% saline solution followed by 4% paraformaldehyde in PBS 2 days after the final in vivo MRI. The spinal cords were removed, postfixed overnight in 4% paraformaldehyde in PBS and left for one day in PBS containing 30% sucrose. Sagittal 35 µm thick sections of the thoracic spinal cord containing the injured area were cut with a cryostat. Every seventh section was mounted immediately on glass slides for Nissl staining. In the remaining sections, Prussian blue staining and light level immunohistochemistry was performed for a more detailed morphological analysis of the contused spinal cord tissue. Prussian blue staining, which was employed to detect hemosiderin deposits, was performed as follows: sections mounted on gelatin coated slides were immersed in a solution of 4% potassium ferrocyanide and 4% HCl for 15 min. After several rinses sections were counterstained with Vector Nuclear Fast Red solution (Linaris, Wertheim, Germany) for 5 min and dehydrated before coverslip

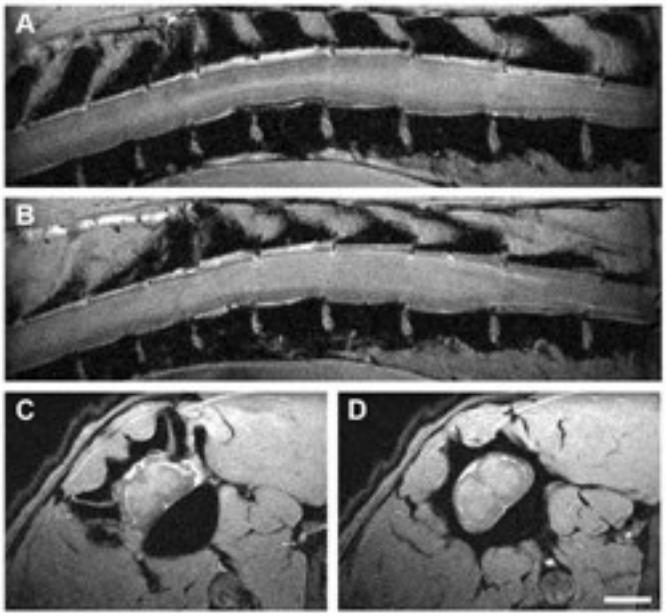

Figure 1: *In vivo MRI of intact spinal cord at 17.6 T.* A,B *show sagittal scans through the thoracic spinal cord. Acquisition parameters: slice thickness 239 µm, FOV 40 x 30 mm, in plane resolution 156 x 117 µm, TR approx. 200 ms (depending on heart rate), TE 4.4 ms.* C,D *display axial scans through the thoracic spinal cord. Acquisition parameters: slice thickness 500 µm, FOV 17.7 x 35.5 mm, in plane resolution 69x69 µm, TR and TE as above. Scale bar 2 mm (A) A more lateral sagittal scan depicts primarily white matter (lower signal) with some longitudinally oriented more hyperintense structure, reflecting the gray matter of the lateral ventral horn. Cerebrospinal fluid appears hyperintense, vertebral bodies are hypointense. (B) Most of the spinal cord parenchyma displayed here represents gray matter (hyperintense) surrounded by white matter tracts (hypointense) in a paramedian sagittal scan through the spinal cord. (C) An axial scan through the thoracic spinal cord allows the clear distinction between the typical butterfly appearance of the spinal cord gray matter and the surrounding hypointense white matter. Also of note, spinal roots can be clearly identified at this level. (D) A subsequent scan more caudally shows the spinal cord in cross-section away from the spinal root entry zone.*

ping with Neo Mount (Merck, Darmstadt, Germany). For immunohistochemistry, the following primary antibodies were used: mouse-anti-GFAP (for astrogliosis; DAKO, Glostrup, Denmark; at 1/2000), goat-anti-collagen type III (for the fibrous scar; Southern Biotechnology, Birmingham, USA, at 1/100) and mouse anti-rat monocytes/macrophages (clone ED1; Chemicon, Hofheim, Germany, at 1/1000). The sections were blocked in TBS + 3% donkey serum + 0.1% Triton-X, and incubated with the primary antibody in TBS + 3% donkey serum + 0.1% Triton-X overnight at 4°C on a rotating platform. The following day, sections were incubated with the secondary antibody (biotinylated donkey IgG, Jackson, Hamburg, Germany; at 1/1000) in TBS containing 3% donkey serum + 0.1% Triton-X. Sections were incubated with avidin-biotinylated-peroxidase complex (Vector Elite kit; Linaris, Wertheim, Germany) followed by development for 3–15 min in a 0.05% solution of 3,3'-diaminobenzi-

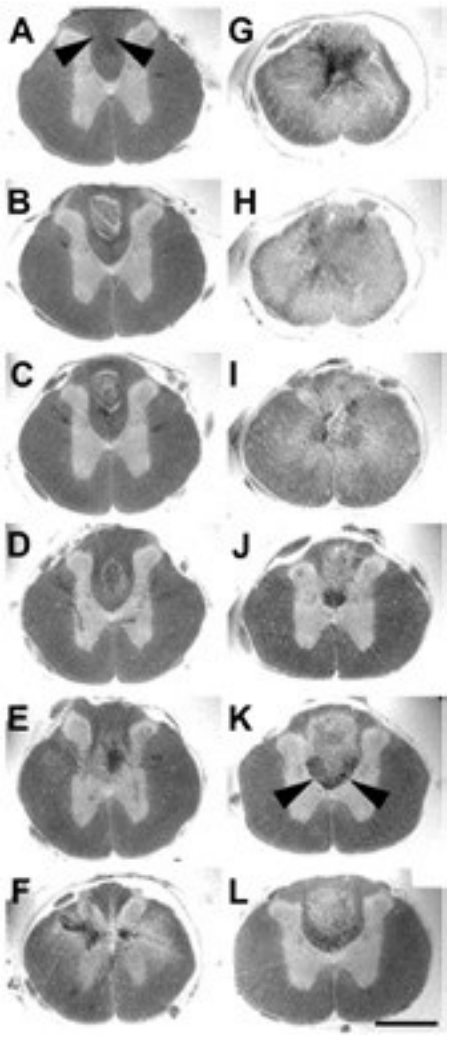

Figure 2: *Axial ex vivo MRI scans of contused rat spinal cord. Axial slices of ex vivo MRI show microscopy grade visualization of morphological changes in the injured rat spinal cord 4 weeks after contusion injury at midthoracic level. Acquisition parameters: 2D multi-slice spin echo, slice thickness 300 µm, FOV 6x6 mm, in plane resolution 23 x 23 µm, TE 7.5 ms, TR 2 s. Scale bar 1 mm.* A-L *show consecutive sections in the rostral-caudal direction. In rats the dorsal columns contain not only ascending proprioceptive projections, which are located in the dorsal half of the dorsal column. The crossed corticospinal tract projects in the ventral half of the dorsal columns, unlike humans, where the majority of corticospinal axons are located in the lateral columns. (A-F) In sections rostral to the contusion site, the spinal cord morphology is still maintained with a clear differentiation of white and gray matter. Note the loss of signal in the dorsal part of the dorsal columns (arrowheads) identical with ascending proprioceptive projections. (G-I) At the lesion center, the spinal cord diameter is reduced, and gray and white matter can no longer be separated. Hypointensities located in the center (G) reflect hemosiderin deposits. (J-L) Caudal to the lesion, the gray-white matter contrast is preserved. Both in rostral and caudal scans (B-D,J-L) hyperintense signals are found in the dorsal columns consistent with cystic defects (see also Fig. 3). Hypointensities in axial scans rostral to the lesion correspond to ascending sensory projections, whereas in caudal scans they represent the area of the corticospinal tract (J-L; arrowheads).*

dine (DAB), 0.01% H_2O_2 and 0.04% nickel chloride in TBS yielding a brown-black reaction product. Sections were mounted onto gelatin-coated glass slides, air-dried, dehydrated and coverslipped with Neo Mount (Merck, Darmstadt, Germany). The histological analysis was performed using a Leica DMR microscope equipped with a Spot CCD camera model 2.2.1 (Diagnostic Instruments, Michigan, USA).

3. RESULTS

3.1 In vivo MRI of intact spinal cord

Gradient echo MRI with ECG triggering and respiratory gating yielded high reso - lution images of intact thoracic rat spinal cord in vivo without significant motion arti facts (Fig. 1). The typical butterfly-shaped gray matter could be clearly distinguished from the less intense surrounding white matter axonal tracts. The cerebrospinal fluid surrounding the spinal cord appeared as a small hyperintense rim adjacent to the

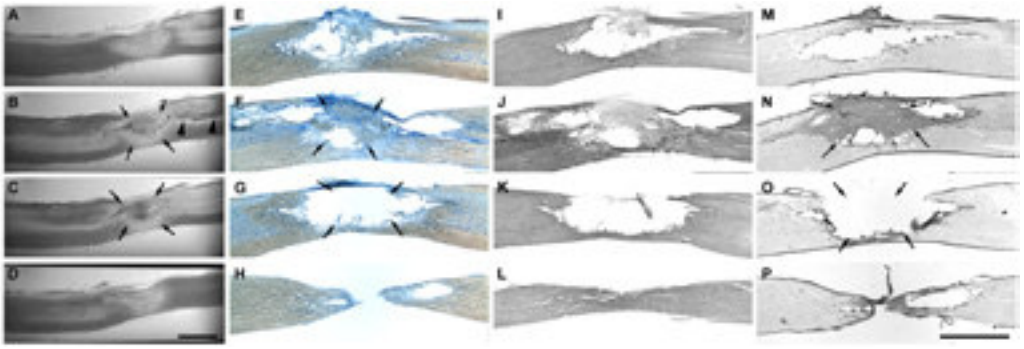

Figure 3: *Sagittal ex vivo MRI scans of contused rat spinal cord and corresponding histology. Midthoracic contusion injury 4 weeks post lesioning, same specimen as Fig. 2. Acquisition parameters: 2D multi-slice spin echo, slice thickness 208 µm, FOV 20x6 mm, in plane resolution 23 x 78 µm, TE 7.5 ms, TR 2 s. Scale bar 2 mm.* A-D *Ex vivo MRI scans from lateral to medial.* E-H *Corresponding Nissl stained sections.* I-L *Corresponding GFAP immunostained sections.* M-P *Corresponding collagen type III immunostained sections. Homogenous hyperintensities at the injury center (A) correspond to cystic lesion defects in histological sections (E,I,M). In other sections. mixed hypo-/hyperintensities in the lesion center (B,C; arrows) are associated either with cystic lesion defects, hemosiderin deposits or fibrotic scar formation (F,N,G,O; arrows). A hypointensity following the path of the dorsal corticospinal tract caudal to the lesion - corresponding to hypointensities in the dorsal columns in axial MR scans (see Fig.2) - is highlighted by arrowheads (B).*

spinal cord due to its longer T_2 and T_2^* relaxation times. With the applied sequence vertebral bodies appeared completely dark, while vertebral disks were bright.

3.2 Ex vivo MRI of contused spinal cord

Spin echo images of excised spinal cord 4 weeks after a thoracic contusion injury revealed a signal pattern away from the injury epicenter in axial slices (Fig. 2), which was almost identical to in vivo gradient echo images in unlesioned animals (Fig. 1 C,D). Gray matter was hyperintense compared to white matter. The central canal could be clearly identified. The gray/white matter differentiation completely vanished at the contusion center (Fig. 2 G,H). The homogenous hyperintense signal, which was pronounced in the spinal cord center and diminished towards the surface of the cord in all directions, was only interrupted by areas of signal loss in the center of the cord, which were confined mostly to the gray matter (Fig.2 G). Trauma induced hemorrhage and consecutive hemosiderin deposits are the likely pathologic correlates for this signal free area, which have been described to occur frequently within the spinal cord gray matter after injury [17]. Hypointensities within the lesion center (in particular in sagittal MR scans) - not as pronounced as the described hemosiderin associated changes - corresponded to immunoreactivity for collagen type III, but not GFAP, in sagittal histological sections (Fig. 3 B,J,N), thus representing components of the fibrous rather than the gliotic scar. The overall diameter of the cord was reduced, in particular the dorsolateral columns were symmetrically diminished in volume (Fig. 2 G,H), reflecting substantial irreversible

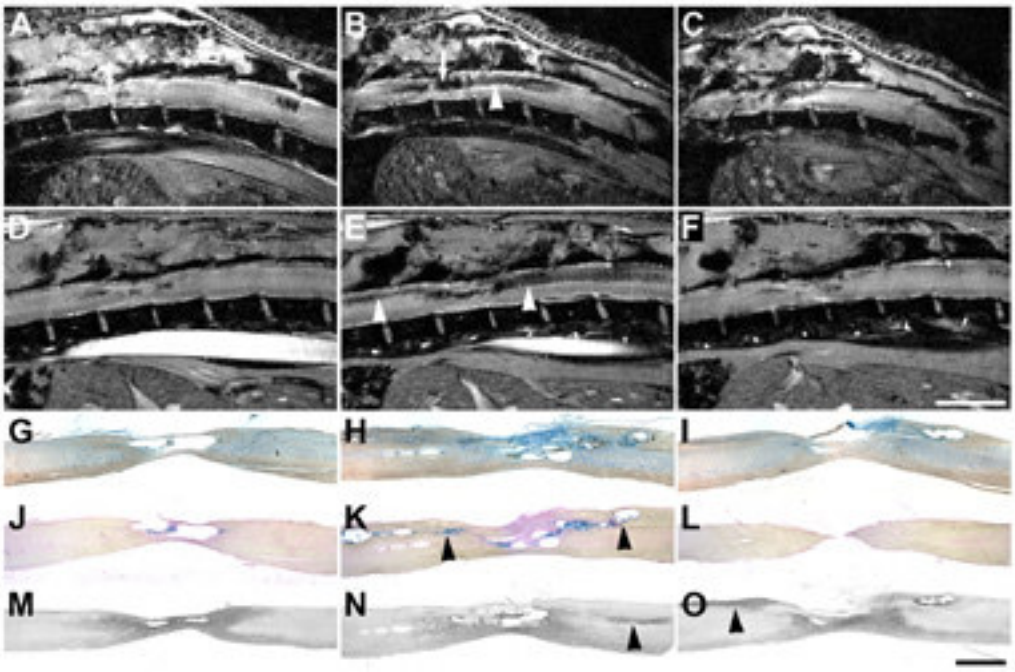

Figure 4: *Sagittal in vivo MRI scans of contused rat spinal cord and corresponding histology. In vivo MRI in adult rats at 2 and 8 weeks after thoracic contusion injury displays signal changes, which parallel the ex vivo MRI data. Acquisition parameters: 2D multi-slice gradient echo,* A-C *slice thickness 311 µm, FOV 30 x 30 mm, in plane resolution 117 x 117 µm, TE 4.4 ms, TR approx. 200 ms (depending on heart rate).* D-F *slice thickness 300 µm, FOV 40 x 25 mm, in plane resolution 156 x 98 µm, TE 3.7 ms, TR 200 ms (depending on heart rate). Scale bar A-F 5 mm, G-O 1 mm. Consecutive sagittal MR scans are shown at 2 weeks (A-C) and 8 weeks (D-F) post injury with corresponding histological Nissl (G-I) and Prussian Blue (J-L) stained sections, and sections processed for ED1 immunohistochemistry (macrophages, monocytes) (M-O), all from the same animal. Arrows in* A,B *highlight the site of the impact. Hypointensities along ascending and descending axon projections in the dorsal columns (B,E) correlate with hemosiderin deposits (K) rather than macrophage/ monocyte infiltration (O) (respective areas are highlighted by arrowheads). These changes increase from 2 weeks (C) until 8 weeks (G) post injury. The clear reduction in cord diameter over time (B versus E; C versus F) corresponds to the atrophy seen in histological sections (G-O).*

atrophy as soon as 4 weeks after injury. In some Nissl stained sections (Fig. 3 G) all types of organized tissue were absent, suggesting a developing fluid-filled cavity. However, corresponding MRI scans did not display a homogenous hyperintensity (Fig. 3 C), which would be the MR equivalent of a cystic lesion defect. Instead, only a small hyperintense band - the correlate of the true cystic lesion defect - surrounded a hypointense core. Thus, it is likely that this hypointense area contained non-organized material (inflammatory cells and cell debris mixed with hemosiderin deposits), which is regularly lost during the process of histological analysis.

Remote from the lesion center, some neuroanatomically restricted signal changes could be observed (Fig. 2 A,J-L; Fig. 3 B). Caudal to the lesion center, hypointensities strictly confined either to the former main dorsal corticospinal tract caudal to

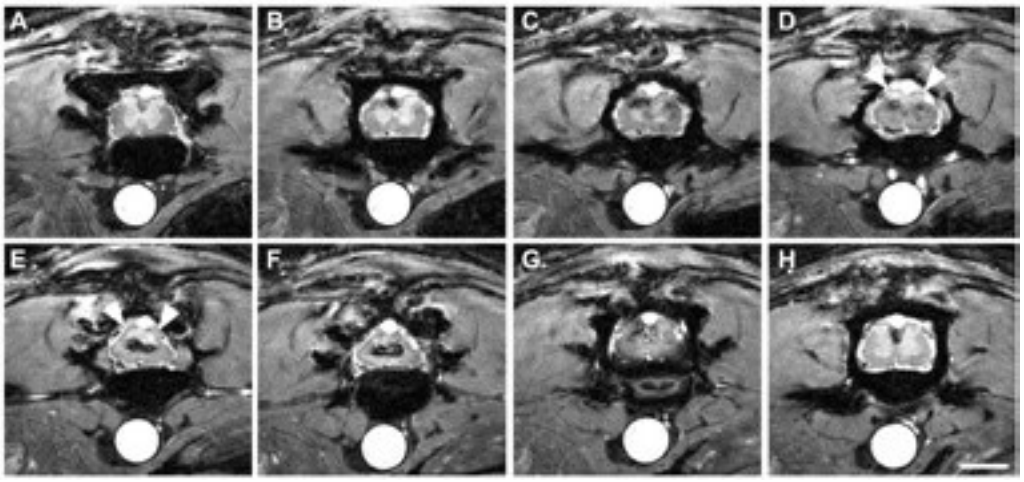

Figure 5: *Axial in vivo MRI scans of contused rat spinal cord. In vivo MR axial scans in adult rats 6 weeks post injury. Acquisition parameters: 2D multi-slice gradient echo, slice thickness 370 µm, FOV 20 x 20 mm, in plane resolution 78 x 78 µm, TE 4.2 ms, TR approximately 200 ms (depending on heart rate). Scale bar 2 mm. Scans rostral to the contusion (A-C), at the lesion center (D-G) and caudal to the lesion (H). The clear differentiation between white and gray matter disappears over subsequent sections. At the lesion center, hypointensities are surrounded by hyperintensities, which are less pronounced towards the cord surface (E,F). The dorsal aspect of the spinal cord at the lesion site appears more homogenously hyperintensive, most likely representing cystic changes (D,E; arrowhead). Signs of atrophy are present in the dorsolateral spinal cord (E,F)*

the lesion or to the ascending proprioceptive pathways (gracile fascicle) rostral to the lesion were identified. Hyperintense regions within the dorsal columns rostrally and caudally (Fig. 2 B-D,J-L; 3 A,B) can be attributed to cystic necrotic zones, which were identified in the corresponding sagittal histological sections (Fig.3 F). There was no difference in overall signal changes compared to the spinal cord sample, which was taken 2 weeks after the contusion injury (data not shown).

3.3 In vivo MRI of contused spinal cord

Five animals with spinal cord contusions at thoracic level applied by the IH Impactor and one intact animal were analyzed with MRI at 2, 6 and 8 weeks postoperatively. Only 2 out of 5 injured animals survived the MR imaging procedure and were thus obtainable for histological evaluation. The majority of signal changes observed in ex vivo spin echo images in the contused spinal cord were almost identical to in vivo gradient echo images of the contused spinal cord. The cord diameter was reduced at the lesion center; in particular, the dorsolateral aspects were atrophic (Fig. 4 A-F; 5 E,F), which was confirmed by identical findings in corresponding Nissl stained histological sections. Towards the lesion epicenter, the gray/white matter differentiation completely vanished (Fig. 5 D-G). The signal pattern of the gray matter in the intact spinal cord (Fig. 1 C,D) was replaced by hypointense areas in the center of the cord surrounded by a hyperintense rim dorsally

Table 2: *A comparison of the different spatial resolution in previous rat spinal cord injury in vivo MRI studies. If one study used different resolutions, the highest resolution is quoted.*

Voxel volume (nl)	In-plane-Resolution (µm)	Slice thickness (µm)	Field strength (T)	Coil type	Reference
2.25	78x78	370	17.6 T	surface coil	present study
12.2	78x156	1000	1.9 T	implanted	[11]
304	780x780	500	1.5 T	surface coil	[12]
17.3	76x76	3000	4.7 T	surface coil	[13]
76	195x195	2000	2.1 T	surface coil	[14]
	not provided	2800	2 T	surface coil	[15]
80	200x200	2000	4.7 T	birdcage coil	[16]
12.7	130x98	1000	2 T	implanted	[17]
8.1	78x104	1000	7 T	implanted	[18]

and ventrally (Fig. 5 D-G). As described in ex vivo MRI (Fig. 2 F,G), the hypointensities at the lesion center represent hemosiderin deposits, which are remnants of the hemorrhage caused by the trauma corresponding to dark areas in Nissl and Prussian Blue stained sections (Fig. 4 K,N). In addition, hypointensities were found confined to the dorsal columns rostral and caudal to the lesion, both in sagittal and axial scans (Fig. 4 B,E; 5 H), which are also paralleled by ex vivo MRI findings. These hypointensities could be correlated with hemosiderin deposits as depicted by Prussian Blue staining of corresponding spinal cord sections (Fig. 4 K). There was no correlation with areas of macrophage/monocyte infiltration (Fig. 4M-O), which are - besides location adjacent to the injury center - commonly identified in white matter tracts remote from the lesion site highlighting areas of ongoing wallerian degeneration (N. Weidner, unpublished observation).

In Nissl stained histological sections (Fig. 4 H), small cigar shaped cystic areas decreasing in size rostrally were identified, which represent areas of beginning post-traumatic syrinx formation. In in vivo MRI, a corresponding signal was not clearly identifiable (Fig.4 B,E). Most likely, the chosen sagittal imaging planes did not include the location of the central canal.

4. DISCUSSION

This study was undertaken to evaluate the capabilities of high field (17.6 T) MRI to identify morphological changes occurring after experimental spinal cord contusion injury in adult rats. Findings from this study will serve as a basis for future preclinical experiments employing high field MRI to monitor cell-based regenerative strategies in the injured spinal cord, which might become a relevant therapy for spinal cord injured human subjects.

Thus far, only a few publications are available describing findings of morphological changes obtained by MR imaging in vivo in spinal cord injured rats [11-19]. Of these, only two MRI studies investigated spinal cord contusion injuries [16, 18], which are considered to closely mimic pathomor-

phological changes occurring after spinal cord injury in human subjects. In all previous studies, only a very limited resolution was achieved at field strengths ranging from 1.5 up to 7 T. Lower field strengths limit the achievable spatial resolution due to SNR restrictions. Therefore, in-plane resolution and slice thickness have to be reduced. The best resolution was achieved with implanted coils[11, 17, 18], which improve the SNR compared to surface coils, but require an additional surgical procedure. Despite the use of a surface coil, we were able to achieve a spatial resolution at 17.6 T, which is four times higher than the best previously reported resolution with an implanted coil (Table 2). White and gray matter differentiation[13, 16, 17], the delineation of cyst formation and hemorrhage from surrounding intact spinal cord parenchyma have been reported[13, 17]. However, none of these studies was able to spatially allocate respective signal changes as precise as in the present study. The ability to visualize signal changes at a high spatial resolution will become particularly relevant for future MRI studies employed to track the survival and migration of a small number of paramagnetically labeled transplanted cells in the injured spinal cord in small animals[22]. Both ex vivo and in vivo MRI of injured rat spinal cords consistently depicted hypointensities in the dorsal columns rostral and caudal to the contusion injury at thoracic level. The comparison with corresponding histological sections revealed that these hypointense areas represent hemosiderin deposits due to trauma induced hemorrhage rather than wallerian degeneration, which has also been described to induce hypointensities following spinal cord injury [23]. Both, neuropathological and the neuroradiological studies frequently report structural changes representing hemorrhage following spinal trauma [17, 24, 25]. However, respective changes are observed in the gray matter accentuated in and adjacent to the lesion center. To our knowledge, extensive white matter MRI signal changes representing hemosiderin deposits as observed in the present study have not been described yet. Field strength dependent changes in terms of relaxation rates and the higher spatial resolution seem to have increased the contrast in regions of iron deposition [26], thus allowing visualization of relatively discrete hemosiderin deposits within the spinal cord. Whether the signal changes observed in this animal model of spinal cord injury reflect pathological sequels of this disease condition in humans remains to be determined. In case, hemosiderin deposits reflecting a former hemorrhage are more widespread than previously thought, free radicals accumulating after an intraspinal hemorrhage might further contribute to the poor intrinsic regenerative capacity of the injured mammalian spinal cord[27].

Ex vivo and in vivo MRI results show a mismatch of MR images and corresponding histological sections (Nissl stains) in regard to the extent of cystic defects. In histological sections, we frequently observe a rather large cystic lesion defect upon microscopic analysis, which overestimates the true size of cystic changes. During the preparation of histological sections from

contused spinal cord tissue, non-organized material such as cell debris, macrophages mixed with remnants of previous hemorrhages filling the cyst in part is lost. In contrast, MR signal changes in corresponding areas are much more diverse, displaying not only hyperintensities reflecting cystic degeneration as suggested by histology, but in addition hypointensities representing hemosiderin and cell debris. Thus, in vivo visualization by MRI provides invaluable additional information, which cannot be obtained from histological examination. For example, it is extremely important to differentiate between these alterations in cell transplantation approaches. Transplanting cells in a milieu rich in inflammatory cells and hemosiderin will decrease the survival rate of transplanted cells, thus jeopardizing the transplantation success [28]. Analyzing these changes over time using MRI will help to establish the optimal timing and location for transplantation after injury.

A significant limitation for small animal imaging at 17.6 T at this point is the reported poor survival rate of rats induced by the scanning procedure. Even though a custom-built probe head was used to overcome spatial restrictions[21], the tight fitting of experimental animals can sometimes lead to insufficient air circulation resulting in a rise of the isoflurane concentration around the animal. Furthermore the gradient cooling unit was maintained at 37°C ± 2°C throughout the imaging protocol to keep the animal at body temperature. Since only the temperature of the gradient cooling unit, but not the actual body temperature of the animals, was monitored, it is conceivable that the temperature of the animal was beyond physiological levels, thus contributing to the observed mortality. The present study was conducted to investigate the capabilities of high field MRI to monitor structural changes occurring after spinal cord injury in rats. Results demonstrate that MR imaging at 17.6 T using a surface coil provides extremely high-resolution visualization of structural changes occurring in the rat spinal cord following a contusion injury ex vivo and in vivo, which is superior to the best known spatial resolution even with implantable coils. The achieved spatial resolution allows to exactly localize morphological changes such as cyst formation and hemosiderin deposition, which are sometimes not even seen with histological analysis of spinal cord injured animals over time. In principle, in vivo high resolution MRI should allow repeated structural analysis in individual animals, which would also help to significantly reduce the number of animals required for preclinical investigations. However, the problem of poor animal survival during MR imaging needs to be solved.

5. ACKOWLEDGEMENTS

This study was supported by Deutsche Forschungsgemeinschaft (Ha 1232/13). We would like to thank S. Aussenhofer and M. Caioni for expert technical assistance. We also would like to thank V. Herold and E. Rommel for helpful discussions throughout the course of this study and N. Seiberlich for helpful comments on the manuscript.

6. REFERENCES

1. Manelfe, C. Imaging of the spine and spinal cord. Curr Opin Radiol 3, 5-15 (1991).
2. Hadley, D. M. & Teasdale, G. M. Magnetic resonance imaging of the brain and spine. J Neurol 235, 193-206 (1988).
3. Flanders, A. E., Spettell, C. M., Tartaglino, L. M., Friedman, D. P. & Herbison, G. J. Forecasting motor recovery after cervical spinal cord injury: value of MR imaging. Radiology 201, 649-55 (1996).
4. Grill, R., Murai, K., Blesch, A., Gage, F. H. & Tuszynski, M. H. Cellular delivery of neurotrophin-3 promotes corticospinal axonal growth and partial functional recovery after spinal cord injury. J Neurosci 17, 5560-72 (1997).
5. Xu, X. M., Guenard, V., Kleitman, N. & Bunge, M. B. Axonal regeneration into Schwann cell-seeded guidance channels grafted into transected adult rat spinal cord. J Comp Neurol 351, 145-60 (1995).
6. Li, Y., Field, P. M. & Raisman, G. Repair of adult rat corticospinal tract by transplants of olfactory ensheathing cells. Science 277, 2000-2 (1997).
7. Liu, Y. et al. Transplants of fibroblasts genetically modified to express BDNF promote regeneration of adult rat rubrospinal axons and recovery of forelimb function. J Neurosci 19, 4370-87 (1999).
8. Ramon-Cueto, A., Cordero, M. I., Santos-Benito, F. F. & Avila, J. Functional recovery of paraplegic rats and motor axon regeneration in their spinal cords by olfactory ensheathing glia. Neuron 25, 425-35 (2000).
9. Teng, Y. D. et al. Functional recovery following traumatic spinal cord injury mediated by a unique polymer scaffold seeded with neural stem cells. Proc Natl Acad Sci U S A 99, 3024-9 (2002).
10. Pfeifer, K., Vroemen, M., Blesch, A. & Weidner, N. Adult neural progenitor cells provide a permissive guiding substrate for corticospinal axon growth following spinal cord injury. Eur J Neurosci 20, 1695-704 (2004).
11. Ford, J. C. et al. A method for in vivo high resolution MRI of rat spinal cord injury. Magn Reson Med 31, 218-23 (1994).
12. Guizar-Sahagun, G. et al. Magnetic resonance imaging of the normal and chronically injured adult rat spinal cord in vivo. Neuroradiology 36, 448-52 (1994).
13. Fraidakis, M., Klason, T., Cheng, H., Olson, L. & Spenger, C. High-resolution MRI of intact and transected rat spinal cord. Exp Neurol 153, 299-312 (1998).
14. Fukuoka, M., Matsui, N., Otsuka, T., Murakami, M. & Seo, Y. Magnetic resonance imaging of experimental subacute spinal cord compression. Spine 23, 1540-9 (1998).
15. Ohta, K., Fujimura, Y., Nakamura, M., Watanabe, M. & Yato, Y. Experimental study on MRI evaluation of the course of cervical spinal cord injury. Spinal Cord 37, 580-4 (1999).
16. Metz, G. A. et al. Validation of the weight-drop contusion model in rats: a comparative study of human spinal cord injury. J Neurotrauma 17, 1-17 (2000).
17. Bilgen, M., Abbe, R., Liu, S. J. & Narayana, P. A. Spatial and temporal evolution of hemorrhage in the hyperacute phase of experimental spinal cord injury: in vivo magnetic resonance imaging. Magn Reson Med 43, 594-600 (2000).
18. Narayana, P. A., Grill, R. J., Chacko, T. & Vang, R. Endogenous recovery of injured spinal cord: longitudinal in vivo magnetic resonance imaging. J Neurosci Res 78, 749-59 (2004).
19. Franconi, F., Lemaire, L., Marescaux, L., Jallet, P. & Le Jeune, J. J. In vivo quantitative microimaging of rat spinal cord at 7T. Magn Reson Med 44, 893-8 (2000).
20. Scheff, S. W., Rabchevsky, A. G., Fugaccia, I., Main, J. A. & Lumpp, J. E., Jr. Experimental modeling of spinal cord injury: characterization of a force-defined injury device. J Neurotrauma 20, 179-93 (2003).
21. Behr, V. C. et al. High-resolution MR imaging of the rat spinal cord in vivo in a wide-bore magnet at 17.6 Tesla. Magma (2004).
22. Stroh, A. et al. In vivo detection limits of magnetically labeled embryonic stem cells in the rat brain

using high-field (17.6 T) magnetic resonance imaging. Neuroimage 24, 635-45 (2005).
23. Kuhn, M. J., Johnson, K. A. & Davis, K. R. Wallerian degeneration: evaluation with MR imaging. Radiology 168, 199-202 (1988).
24. Tator, C. H. & Koyanagi, I. Vascular mechanisms in the pathophysiology of human spinal cord injury. J Neurosurg 86, 483-92 (1997).
25. Holtz, A., Nystrom, B., Gerdin, B. & Olsson, Y. Neuropathological changes and neurological function after spinal cord compression in the rat. J Neurotrauma 7, 155-67 (1990).
26. Schenck, J. F. & Zimmerman, E. A. High-field magnetic resonance imaging of brain iron: birth of a biomarker? NMR Biomed 17, 433-45 (2004).
27. Petzold, A. et al. Axonal pathology in subarachnoid and intracerebral hemorrhage. J Neurotrauma 22, 407-14 (2005).
28. Okano, H. et al. Transplantation of neural stem cells into the spinal cord after injury. Semin Cell Dev Biol 14, 191-8 (2003).